Superstructure Multi-objective Techno-economic and Environmental Optimization for the Decarbonization of a Chocolate Factory in Brazil

Leonardo Rodrigues de Araujo[a], Rodrigo Fiorotti[b], Helder Roberto de O. Rocha[c], José Joaquim C. S. Santos[c], Antonio Marco Pantaleo[d,f], José Manuel B. M. Ribeiro[e], Márcio Santos[e] and Christos N. Markides[f]

[a] Federal Institute of Espírito Santo, Vitória, Brazil, leoaraujo@ifes.edu.br, CA
[b] Federal Institute of Espírito Santo, São Mateus, Brazil, rodrigo.fiorotti@ifes.edu.br,
[c] Federal University of Espírito Santo, Vitória, Brazil, helder.rocha@ufes.br, jose.j.santos@ufes.br,
[d] Università degli Studi di Bari Aldo Moro, Bari, Italy, antonio.pantaleo@uniba.it,
[e] University of Coimbra, Coimbra, Portugal, jose.baranda@dem.uc.pt, marcio.santos@dem.uc.pt,
[f] Imperial College London, London, England, c.markides@imperial.ac.uk, a.pantaleo@imperial.ac.uk,

Abstract:

Energy demand in food processing is a major cost driver and a primary source of global carbon emissions. This study investigates the optimal structural and parametric energy system for decarbonization of a chocolate factory utility in Brazil, through a superstructure-based multi-objective approach. The baseline plant relies on electricity purchased from the grid (3.19 MW) for cooling demand (13.4 MW) and natural gas (2,98 MW) for heating demand (2.49 MW), resulting in a separated architecture to produce chilled and hot water, based on chillers and heat exchangers, respectively, without integration between systems. To improve the overall performance, a superstructure-based optimization framework is proposed, integrating a natural gas fired organic Rankine cycle (ORC) generation system with a vapor compression refrigeration (VCR) system, while keeping the existing electric chillers, heat exchangers and boilers. The thermodynamic, economic, and environmental models are implemented in Python using parametric correlations, and the resulting problem is formulated as a nonlinear multi-objective optimization problem in which both structural and operational decision variables are optimized, simultaneously, enabling endogenous configuration selection through implicit activation of these technologies. The optimization method minimizes total cost of energy and simple payback, while maximizing avoided CO_2 emissions. The problem is solved using a Modified Multi-Objective Harris Hawks Optimization algorithm (MMHHO). The solution resulted in a synergistic combination of both process electrification and ORC-VCR system, minimizing exergy destruction in heat exchangers and integrating cooling and heating production, in which the VCR supplies 7.69% and 57.68% of the cooling and heating demand, respectively, and the ORC generates 5,36% of the electricity demand. The total energy demand and emissions reduction are of 26.32% and 46.14%, respectively. Natural gas reduction is of 53%. The proposed framework provides a robust decision-support tool for design of integrated low-carbon industrial energy systems, offering insights into economic and thermodynamic limits for process electrification, with exergy efficiency strategies.

Keywords:

Decarbonization; Electrification; Organic Rankine Cycle; Heat Pumps; Superstructure; Multi-objective Optimization, Chocolate Factory.

1. Introduction

The industrial sector faces the dual challenge of sustaining increasing energy demand while complying with stringent decarbonization targets. In particular, food-processing industries are characterized by simultaneous heating and cooling demands, typically supplied by electrically driven refrigeration systems and fossil-fuel-based boilers, resulting in fragmented energy architectures, significant exergy destruction and high carbon intensity [1,2]. In this context, the transition toward electrified and integrated energy systems has emerged as a critical pathway for reducing industrial emissions, although it introduces additional challenges related to system integration, operational flexibility and dependence on grid electricity [3,4]. On the other hand, organic Rankine cycle (ORC) systems have gained significant attention as a solution for converting low- and medium-grade heat into electrical power, thereby enhancing the overall utilization of thermal energy resources [5,6].

Some studies have demonstrated that ORC systems can achieve competitive performance when properly integrated within industrial energy systems [7,8]. Despite these advances, the optimal integration and sizing of hybrid energy systems combining heat pumps and ORC units remain challenging due to interactions among subsystems and inherent trade-offs between capital cost, operating cost, and environmental performance [9,10]. These challenges are particularly relevant in food-processing industries, where energy systems must simultaneously satisfy multiple thermal and electrical demands under strict economic constraints [11,12].

Specifically, with reference to the same chocolate factory utilities of this work, a recent study on the decarbonization of this industry proposed three alternative scenarios and compared their performance with the current plant, considering a 4E analysis (energy, exergy, environmental, and economic). More details of this study are summarized in Section 2. Although the obtained results demonstrated that full electrification of heating and cooling processes, using a new Vapor Compression Refrigeration (VCR) to simultaneously supply total hot-water and partial chilled-water demand, with electricity from the grid, was the best option, a question arises: do only these three scenarios represent all the possibilities of combination and integration of ORC and VCR for cooling and heating? Of course not! The main limitations of this study are presented in Section 2.

To overcome these limitations, this present work proposes a superstructure-based multi-objective optimization framework. The application of multi-objective optimization techniques has significantly advanced the design and operation of industrial energy systems. Evolutionary algorithms, particularly the Non-dominated Sorting Genetic Algorithm II (NSGA-II), have been widely applied to address conflicting objectives such as cost, efficiency, and emissions [13-15]. In the context of industrial applications, multi-objective optimization has been successfully applied to the integration of heat pumps, combined cooling, heating, and power systems, and process integration problems, demonstrating significant improvements in both thermodynamic and economic performance [11-15]. More broadly, the multi-objective optimization of ORC systems and hybrid configurations combining ORC and heat pumps has been extensively investigated, typically considering objectives such as thermal efficiency, exergy efficiency, heat recovery and economic performance [5–10].

The proposed model integrates a vapor-compression refrigeration (VCR) system operating as an industrial heat pump to an organic Rankine cycle (ORC) for both heat and power generation. Thermodynamic, economic, and environmental models are implemented using first-principles formulations and parametric correlations and the resulting problem is formulated as a nonlinear multi-objective optimization in which both the structural and operational decision variables are optimized, simultaneously. This optimization, simultaneously, minimizes total cost rate and simple payback, while maximizing avoided CO_2 emissions. A Modified Multi-Objective Harris Hawks Optimization algorithm (MMHHO) algorithm is employed.

2. Plant Description and Recent Study

The proposed chocolate plant utility system operates with grid electricity to supply chilled water demand and natural gas to produce steam for hot water demand. The chilled water is delivered by 9 vapor-compression chillers with a total capacity of 13,408 kW and an average coefficient of performance (COP) of 4.26, requiring approximately 3,192 kW of electricity power. Process heating is generated by natural gas boilers operating at a thermal efficiency of 88%, to produce approximately 2,625 kW of saturated steam at 9 bar. The produced steam supplies 24 heat exchangers, producing approximately 2,495 kW of hot water at 56.3 °C. The left side diagram in Figure 1 represents the production of chilled and hot water. The current configuration is an independent heating and cooling production, leading to exergy destruction in heat exchangers, together with fossil fuel and grid electricity dependence for heating and cooling processes.

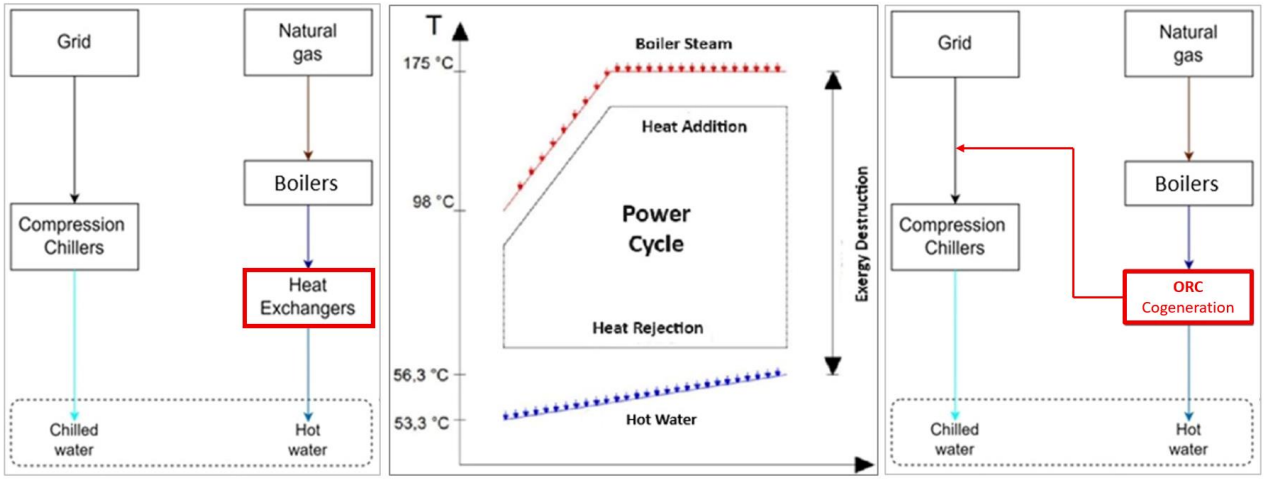

Figure. 1. *Flow chart of the existing system (left side), of the proposed ORC integration (right side) exergy destruction in the heat exchangers (middle) that can be avoided with the ORC cycle*

Figure 1 represents the total exergy destruction in the heat exchangers. A recent study [13] calculated the exergy destruction in the heat exchangers and demonstrated that 71% of the steam exergy produced in the boilers is destroyed in the heat exchangers and proposed their replacement by an ORC Cogeneration, producing additional electricity to reduce the dependence on grid electricity, as shown in the right side diagram in Figure 1. Although the ORC Cogeneration is an alternative to improve de exergy efficiency, in this case, due to the low temperature of the heating demand, the inclusion of a VCR system, to produce simultaneously hot water and chilled water, can significantly enhance the overall system efficiency.

A previous study [13] evaluated each of the three scenarios in Figure 2, considering a 4E analysis (energy, exergy, environmental, and economic). The results, compared with the existing configuration (Scenario A), revealed that Scenario C is the best one, with a VCR, without ORC, in which the VCR produces simultaneously the total hot-water and partial chilled-water demand, with 3,457 kW from the grid, eliminating the natural gas, reducing both total energy demand (44%) and equivalent CO_2 emissions (54%).

Regarding the two scenarios that considered an ORC fuelled by steam from the natural gas boilers, to generate electricity only (Scenario B) or to produce electricity and hot water (Scenario D), from the thermodynamic and environmental point of view, the worst one was electricity-only generation (Scenario B), while the electricity and hot water production (Scenario D) showed no significant advantages or disadvantages. However, the only economically viable scenario was total electrification (Scenario C), eliminating the natural gas boilers and ORC.

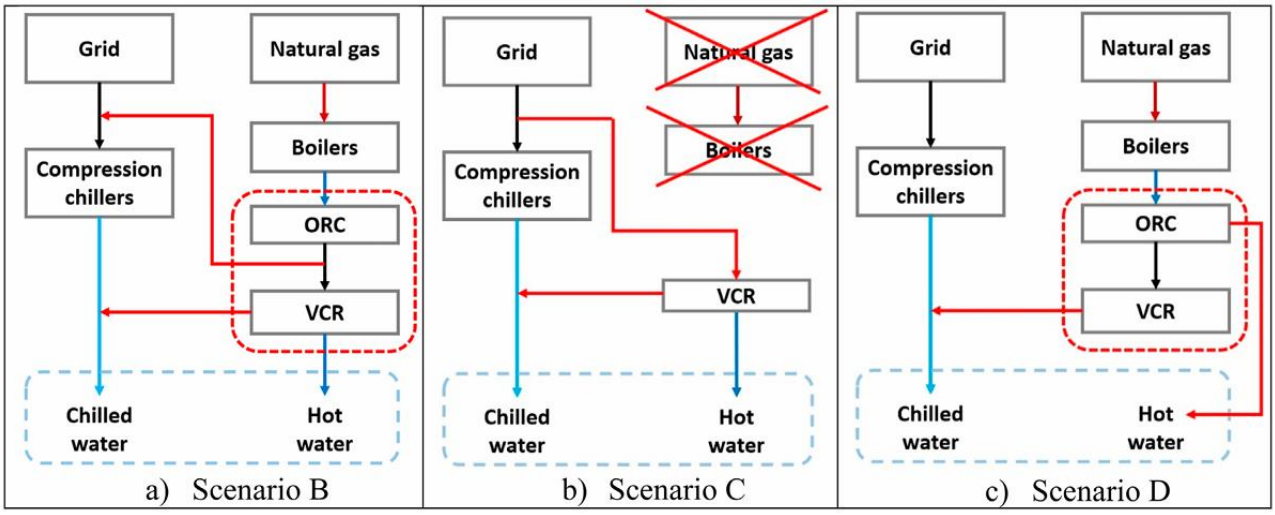

Figure. 2. *Proposed Alternative Scenarios for 4E Evaluation*

Although the exergy diagnosis has shown that the overall thermodynamic efficiency of the plant could increase with the inclusion and integration of an ORC and a VCR (producing hot and chilled water, simultaneously), none of the evaluated alternative scenarios allowed both systems produce two products simultaneously. A scenario was missing where both the ORC and the VCR produce hot water, since in Scenario B only the VCR produces the total hot water and in Scenario D only the ORC produces it.

However, instead of defining several scenarios in order to evaluate which is the best one, the most effective methodology is to define a superstructure representing various scenarios and to perform a structural and parametric optimization to define the best combination of scenarios.

3. Materials and Methods

The methodology consists of a superstructure definition and modelling for subsequent formulation of the multi-objective optimization problem to obtain the optimum thermo-economic-environmental structure.

3.1. Superstructure Description

Figure 3 represents both the process and the physical diagram of the defined energy superstructure, which integrates a new industrial heat pump system based on a vapor-compression refrigeration cycle (VCR) and a new organic Rankine cycle cogeneration system (ORC), both interconnected with the existing compression chillers, the electricity from the grid, natural gas boilers and the heat exchangers, in a superstructure to attend, in a combined way, all the cooling and heating demand of the factory, i.e., all hot and chilled water demand. The hot water demand can be supplied by the existing heat exchangers and by the VCR and ORC condensers, while the chilled water demand can be produced in the existing compression chillers and in the VCR evaporator. The natural gas boilers can supply steam to the ORC evaporator and to the existing heat exchangers.

In addition to being able to generate hot water, the ORC system can also generate electricity, avoiding exergy destruction in the existing heat exchangers and reducing the electricity demand from the electric grid. This ORC dual function creates a direct coupling between fossil fuel efficient use, exergy efficiency and on-site electricity generation, constituting the central thermodynamic interaction of the proposed architecture. Additionally, the dual-purpose of the VCR allows the combined electrification of cooling and heating demands.

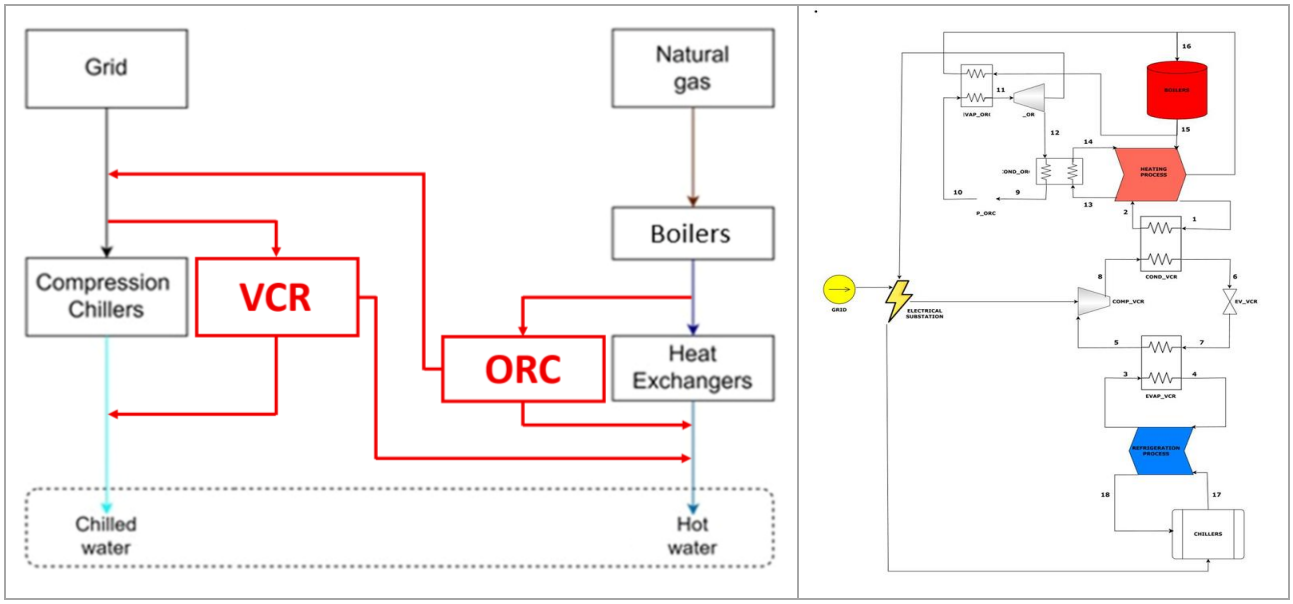

Figure. 3. *Superstructure Productive and Physical Diagram*.

3.2. Superstructure Modelling and Optimization

The thermodynamic modelling of the superstructure considers the existing components as black boxes, as shown in the second diagram in Figure 3, which represents the physical flowsheet of the superstructure and the thermal energy diagram used for mass and energy balance. To estimate the electricity demand from the grid, the existing compression chillers attend the total chilled water demand of 13,408 kW, with an average COP of 4.26, producing chilled water with a temperature differential of 6°C, ranging from13°C to 7°C. For the calculation of the natural gas consumption, the installed steam generation capacity of the natural gas boilers is 9,843 kW and the average thermal efficiency is 88%, producing saturated steam at 9 bar with feed water at 98°C. The heat exchangers supply 2,495 kW of hot water at 56,3 °C, with feed water received at 53.3°C. However, due to significant heat losses, only 83.6 % of the natural gas energy is effectively converted into hot water demand.

For the integrated energy superstructure, according to the second diagram in Figure 3, with the inclusion and interconnection of both ORC and VCR, which are modelled as thermodynamic cycles, the thermodynamic modelling is formulated through the first law of thermodynamics for mass and energy balance, real-fluid properties, and LMTD heat exchanger models. The kinetic and potential effects, pressure drops, and heat losses are neglected for thermodynamic coherence and computational tractability in the multi-objective optimization.

The optimization problem is formulated with continuous decision variables $\mathbf{x} = [\Delta T_{\text{evap,VCR}},\ \Delta T_{\text{cond,VCR}},\ \dot{Q}_{\text{cond,VCR}},\ PP_{\text{evap,ORC}},\ PP_{\text{cond,ORC}},\ \dot{Q}_{\text{cond,ORC}}]^{\text{T}}$, which govern both design conditions and structural activation. Subsystems are activated for $\dot{Q}_{\text{cond}} > 0$ and vanish otherwise, enabling smooth endogenous configuration selection. The process heat demand $\dot{Q}_{\text{proc}} = 2{,}495\ \text{kW}$ is always satisfied, with boiler load $\dot{Q}_{\text{boiler}} = \dot{Q}_{\text{proc}}/0.95 - \dot{Q}_{\text{cond,VCR}} - \dot{Q}_{\text{cond,ORC}} + \dot{Q}_{\text{evap,ORC}}$. This relation reveals a key trade-off: while the VCR reduces the heating demand, ORC activation introduces additional thermal load, implying $\dot{Q}_{\text{boiler}} > 0$ when active. Grid electricity and conventional chillers remain active, ensuring demand satisfaction and reinforcing the hybrid nature of the system. In the VCR model, the decision variables are the terminal temperature differences in the evaporator and condenser $(\Delta T_{evap,VCR})$, $(\Delta T_{cond,VCR})$, and the condenser heat duty $(\dot{Q}_{cond,VCR})$, which define operating conditions and the degree of fossil heat substitution. The cycle operates at steady state with R134a [13]. Boundary conditions are $T_{cw,in} = 326.45\ \text{K}$, $T_{cw,out} = 329.45\ \text{K}$, $T_{chw,in} = 286.15\ \text{K}$, $T_{chw,out} = 280.15\ \text{K}$, and $P_w = 3 \times 10^5\ \text{Pa}$. Efficiencies are $\eta_{c,VCR} = 0.75$ and $\eta_{ger,VCR} = 0.95$, with heat-transfer coefficients $U_{evap,VCR} = 966\ \text{W m}^{-2}\ \text{K}^{-1}$ and $U_{cond,VCR} = 1124\ \text{W m}^{-2}\ \text{K}^{-1}$. The variables are obtained with the relations in Eqs. (1)–(4).

$$T_{evap,\mathrm{VCR}} = T_{chw,out} - \Delta T_{evap,\mathrm{VCR}} \quad (1)$$

$$T_{cond,\mathrm{VCR}} = T_{cw,out} + \Delta T_{cond,\mathrm{VCR}} \quad (2)$$

$$A_{heat\ exchanger,\mathrm{VCR}} = \frac{\dot{Q}_{heat\ exchanger,\mathrm{VCR}}}{U_{heat\ exchanger,\mathrm{VCR}} \cdot \Delta TML_{heat\ exchanger,\mathrm{VCR}}} \quad (3)$$

$$\dot{W}_{c,\mathrm{VCR}} = \dot{m_{VCR}} . (h_8 - h_5) \quad (4)$$

Heat exchanger costs are estimated with Bare-Module factors Eq. (5) using K_j and B_j [16], assuming $F_{M,j} = F_{P,j} = 1.0$ and cost updated is calculated Eq. (6). Compressor cost is obtained with $F_{\mathrm{BM,comp}} = 2.8$. The updated compressor cost is calculated using Eq. (7). The total cost rate is calculated in Eq. (8) using $i = 0.10$ yr^{-1}, $n = 20$ yr, $H = 8{,}760$ h yr^{-1}, and $\phi = 1.06$ [17].

$$F_{BM,j,\mathrm{VCR}} = B_{1,j} + B_{2,j}(F_{M,j}F_{P,j}) \quad (5)$$

$$C_{HX,j,\mathrm{VCR}}^{(2024)} = (10^{K_{1,j}+K_{2,j}log10(A_{j,VCR})+K_{3,j}[log10(A_{j,VCR}]2} \cdot F_{BM,j,\mathrm{VCR}} \cdot f_{FC}) \left(\frac{CEPCI_{2024}}{CEPCI_{2001}}\right) \quad (6)$$

$$C_{comp,\mathrm{VCR}}^{(2024)} = (10^{K_{1,comp}+K_{2,comp}\log_{10}(W_{c,\mathrm{VCR}}^{(kW)})+K_{3,comp}\left[\log_{10}(W_{c,\mathrm{VCR}}^{(kW)})\right]^2} \cdot F_{BM,comp} . f_{FC}) \left(\frac{CEPCI_{2024}}{CEPCI_{2001}}\right) \quad (7)$$

$$\dot{C}_{\mathrm{VCR}} = \frac{C_{HX,j,\mathrm{VCR}}^{(2024)} \cdot \left(\frac{i(1+i)^n}{(1+i)^n-1}\right) \cdot \phi}{H} + \frac{C_{comp,\mathrm{VCR}}^{(2024)} \cdot \left(\frac{i(1+i)^n}{(1+i)^n-1}\right) \cdot \phi}{H} \quad (8)$$

ORC subsystem is modeled with *n*-pentane using CoolProp, operating under evaporation and condensation conditions defined by thermal sources and pinch constraints [13], with temperatures given in Eqs. (9)–(10), while the net output is defined in Eq. (11). Expansor cost is estimated in Eq. (12) with coefficients $K_1 = 2.2476$, $K_2 = 1.4965$, $K_3 = -0.1618$ [16], using $F_{\mathrm{BM}} = 3.5$ and $F_{\mathrm{fees}} = 1.18$, heat exchanger in Eq. (13)-(14) and the pump costs are given in Eq. (15) where $B_1 = 1.89$, $B_2 = 1.35$, $K_1 = 3.3892$, $K_2 = 0.0536$, $K_3 = 0.1538$, $C_1 = -0.3935$, $C_2 = 0.3957$, $C_3 = -0.00226$, and $F_M = 1.6$. The ORC cost rate is obtained in Eq. (16) [17].

$$T_{\mathrm{evap,ORC}} = T_{\mathrm{evap,in}} - PP_{\mathrm{evap,ORC}} \quad (9)$$

$$T_{\mathrm{cond,ORC}} = T_{\mathrm{cond,out}} + PP_{\mathrm{cond,ORC}} \quad (10)$$

$$\dot{W}_{\mathrm{net,ORC}} = \dot{W}_{e,\mathrm{ORC}} - \dot{W}_{p,\mathrm{ORC}} \quad (11)$$

$$C_{e,ORC}^{(2024)} = F_{\mathrm{fees}} \cdot F_{BM} . 10^{K_1+K_2\log_{10}(W_{e,\mathrm{ORC}})+K_3[\log_{10}(W_{e,\mathrm{ORC}})]^2} . \frac{\mathrm{CEPCI}_{2024}}{\mathrm{CEPCI}_{2001}} \quad (12)$$

$$A_{heat\ exchanger,\mathrm{ORC}} = \frac{\dot{Q}_{heat\ exchanger,\mathrm{ORC}}}{U_{heat\ exchanger,\mathrm{ORC}} \cdot \Delta TML_{,heat\ exchanger,\mathrm{ORC}}} \quad (13)$$

$$C_{HX,j,\mathrm{VCR}}^{(2024)} = (10^{K_{1,j}+K_{2,j}log10(A_{j,VCR})+K_{3,j}[log10(A_{j,VCR}]2} \cdot F_{BM,j,\mathrm{VCR}} \cdot f_{FC}) \left(\frac{CEPCI_{2024}}{CEPCI_{2001}}\right) \quad (14)$$

$$C_{P,\mathrm{VCR}}^{(2024)} = 10^{K1,p+K2,plog10(Pp)+K3,p[log10(Pp)]2[B1,p+B2,pFM,p10(C1,p+C2,plog10(Pp)+C3,p[log10(Pp)]2)]} . \left(\frac{CEPCI_{2024}}{CEPCI_{2001}}\right) \quad (15)$$

$$\dot{C}_{\mathrm{ORC}} = \frac{C_{e,ORC}^{(2024)} \cdot \left(\frac{i(1+i)^n}{(1+i)^n-1}\right) \cdot \phi}{H} + \frac{C_{HX,j,\mathrm{ORC}}^{(2024)} \cdot \left(\frac{i(1+i)^n}{(1+i)^n-1}\right) \cdot \phi}{H} + \frac{C_{P,\mathrm{ORC}}^{(2024)} \cdot \left(\frac{i(1+i)^n}{(1+i)^n-1}\right) \cdot \phi}{H} \quad (16)$$

The refrigeration system consists of nine parallel electric chillers supplying $Q_{\mathrm{ch,base}} = 13{,}408$ kW, operating at $T_{\mathrm{chw,in}} = 286.15$ K, $T_{\mathrm{chw,out}} = 280.15$ K, and $P_w = 3 \times 10^5$ Pa, with $COP_{\mathrm{ch}} = 4.26$ [13]. With the VCR contribution $\dot{Q}_{\mathrm{evap,VCR}}$ reducing the residual load and the corresponding demand updated in Eq. (17). The net electrical exchange with the grid is defined as the balance between on-site generation and demand (Eq. 18), with positive values indicating net import and generator efficiency η_{GER}. Annual consumption is calculated under continuous operation $\left(H = 8760 \text{ h yr}^{-1}\right)$ in Eq. (19). Energy is allocated into peak and off-peak shares using $f_p = 0.09$ (Eq. 20), with energy charges (TE + TUSD) evaluated in Eq. (20) using tariffs T_p and T_{fp}. Contracted demand and cost are given in Eq. (21) using T_{dem}. The hourly grid cost is calculated in Eq. (23), with $f_x = 5.19$ R$.US^{-1}.

$$\dot{P}_{e,\mathrm{ch}} = \left(\frac{Q_{\mathrm{ch,base}} - \dot{Q}_{evap,\mathrm{VCR}}}{COP_{\mathrm{ch}}}\right) / \eta_{\mathrm{GER}} \quad (17)$$

$$P_{el,grid} = -\frac{\dot{W}_{net,OCR}}{\eta_{\mathrm{GER}}} + P_{el,ch} + \frac{\dot{W}_{c,VCR}}{\eta_{\mathrm{GER}}} \quad (18)$$

$$E_p = \left(1 - f_p\right) E_{grid,yr} = \left(1 - f_p\right) \left(-\frac{\dot{W}_{net,OCR}}{\eta_{\mathrm{GER}}} + P_{el,ch} + \frac{\dot{W}_{c,VCR}}{\eta_{\mathrm{GER}}}\right) . H \quad (19)$$

$$C_{en,yr} = E_p(T_p + b) + E_{fp}(T_{fp}) \quad (20)$$

$$D_{contr} = \left(-\frac{\dot{W}_{net,OCR}}{\eta_{\mathrm{GER}}} + P_{el,ch} + \frac{\dot{W}_{c,VCR}}{\eta_{\mathrm{GER}}}\right) + 1000 \quad (21)$$

$$C_{dem,yr} = D_{contr} . T_{dem} . 12 \quad (22)$$

$$C_{grid,USD/h} = \frac{C_{grid,BRL/h}}{fx} \tag{23}$$

The process-heating subsystem is modeled as a natural-gas-fired boiler supplying the residual demand not covered by VCR and ORC condensers, with $\dot{Q}_{\text{proc,base}} = 2{,}495$ kW and water heated from 53.3 to 56.3 °C [10]. Steam is generated at 9 bar with condensate return at 98 °C, with the steam flow rate given in Eq. (24). Boiler efficiency is $\eta_{\text{cald}} = 0.88$ and global efficiency $\eta_{\text{global}} = 0.836$ [1,14]. Heat fuel input is calculated in Eq. (25). Natural gas consumption is evaluated using $LHV = 47.35$ MJ kg^{-1} and $\rho_{\text{gas}} = 0.76$ kg m^{-3}, and the hourly fuel cost is obtained in Eq. (40) using $T_{\text{gas}} = 0.35$ US$ m^{-3}.

$$\dot{m}_{\text{vapor}} = \frac{\dot{Q}_{\text{boiler}}}{\eta_{\text{proc}}\,\Delta h_{\text{vapor}}} = \tag{24}$$

$$\dot{Q}_{\text{fuel}} = \frac{\dot{Q}_{\text{steam}}}{\eta_{\text{cald}}} = \frac{\dot{m}_{\text{vapor}}\,\Delta h_{\text{vapor}}}{\eta_{\text{cald}}} \tag{25}$$

$$\dot{C}_{\text{gas}} = \frac{\dot{m}_{\text{gas}}}{\rho_{\text{gas}}}.\,T_{\text{gas}} = \frac{\frac{\dot{Q}_{\text{fuel}}}{PCI_{\text{gas}}}}{\rho_{\text{gas}}}.\,T_{\text{gas}} \tag{26}$$

Grid emissions are calculated using the Brazilian SIN emission factor $FE_{\text{grid}} = 0.0289$ kg kWh^{-1}. Avoided grid emissions is calculated in Eq. (27). Boiler emissions are evaluated using the IPCC factor $FE_{\text{NG}} = 56.1$ tCO$_2$ TJ^{-1}, The corresponding avoided boiler emissions are determined in Eq. (28).

$$CO_{2,\text{grid}}^{avoid} = CO_{2,\text{grid}}^{base} - CO_{2,\text{grid}} = \frac{P_{el,\text{ch,base}}\,FE_{\text{grid}}\,H}{1000} - \frac{P_{el,\text{grid}}\,FE_{\text{grid}}\,H}{1000} \tag{27}$$

$$CO_{2,\text{boiler}}^{avoid} = CO_{2,\text{boiler}}^{base} - CO_{2,\text{boiler}} = \left[\left(\dot{m}_{gas}^{base}\,PCI_{gas}\,H\right)\left(\frac{3.6}{10^6}\right)\right]FE_{\text{NG}} - \left[\left(\dot{m}_{gas}\,PCI_{gas}\,H\right)\left(\frac{3.6}{10^6}\right)\right]FE_{\text{NG}} \tag{28}$$

The economic performance of the integrated ORC–VCR system is evaluated using the simple payback adopted $\left(H = 8{,}760 \text{ h yr}^{-1}\right)$. The simple payback is determined in Eq. (29) [17].

$$PB = \frac{I_{\text{tot}}}{C_{\text{op}}^{base} - C_{\text{op}}^{new}} = \frac{C_{\text{VCR}} + C_{\text{ORC}}}{\left(\left(\dot{C}_{\text{grid}}^{base} + \dot{C}_{\text{gas}}^{base}\right).H\right) - \left(\left(\dot{C}_{\text{grid}} + \dot{C}_{\text{gas}}\right).H\right)};\ \left(C_{\text{op}}^{base} - C_{\text{op}}^{new} > 0\right) \tag{29}$$

The decision variables define operating conditions and utilization levels, for the VCR ($\Delta T_{\text{evap,VCR}}$, $\Delta T_{\text{cond,VCR}}$, and $\dot{Q}_{\text{cond,VCR}}$) and for the ORC ($PP_{\text{evap,ORC}}$, $PP_{\text{cond,ORC}}$, and $\dot{Q}_{\text{cond,ORC}}$): $3 \le \Delta T_{\text{evap,VCR}} \le 6, 4 \le \Delta T_{\text{cond,VCR}} \le 8, 0 \le \dot{Q}_{\text{cond,VCR}} \le 2{,}495$ kW; $5 \le PP_{\text{evap,ORC}} \le 20$; $5 \le PP_{\text{cond,ORC}} \le 15$; $0 \le \dot{Q}_{\text{cond,ORC}} \le 2{,}495$ kW.

System performance is evaluated through a multi-objective formulation Eq. (30) with objectives in Eqs. (31)–(33), subject to energy balance constraints (Eqs. 34 and 36), while cooling and electrical balances are given in Eq. (37). This formulation enables simultaneous optimization of structure and operation, capturing nonlinear trade-offs and allowing decarbonization pathways to emerge endogenously.

$$\max f_1(\mathrm{x}), \min f_2(\mathrm{x}), \min f_3(\mathrm{x}) \quad s.t. \tag{30}$$

$$f_1(\mathrm{x}) = \dot{CO}_{2,\text{avoid}}(\mathrm{x}) = \left(\dot{CO}_{2,\text{grid}}^{\text{base}} - \dot{CO}_{2,\text{grid}}(\mathrm{x})\right) + \left(\dot{CO}_{2,\text{boiler}}^{\text{base}} - \dot{CO}_{2,\text{boiler}}(\mathrm{x})\right) \tag{31}$$

$$f_2(\mathrm{x}) = \dot{C}_{\text{tot}}(\mathrm{x}) = \dot{C}_{\text{VCR}}(\mathrm{x}) + \dot{C}_{\text{ORC}}(\mathrm{x}) + \dot{C}_{\text{grid}}(\mathrm{x}) + \dot{C}_{\text{gas}}(\mathrm{x}) \tag{32}$$

$$f_3(\mathrm{x}) = PB(\mathrm{x}) = \frac{C_{\text{VCR}}(\mathrm{x}) + C_{\text{ORC}}(\mathrm{x})}{C_{\text{op}}^{\text{base}} - C_{\text{op}}^{\text{new}}(\mathrm{x})} \text{ for } C_{\text{op}}^{\text{base}} > C_{\text{op}}^{\text{new}}(\mathrm{x}) \tag{33}$$

$$\dot{Q}_{\text{boiler,proc}} \ge \dot{Q}_{\text{proc}}^{\text{base}} - Q_{\text{cond,VCR}}(\mathrm{x}) - \dot{Q}_{\text{cond,ORC}}(\mathrm{x}) \tag{34}$$

$$\dot{Q}_{\text{boiler}}(\mathrm{x}) = \dot{Q}_{\text{boiler,proc}} + \dot{Q}_{\text{evap,ORC}}(\mathrm{x}) \ge 0 \tag{35}$$

$$\dot{Q}_{\text{ch}}(\mathrm{x}) = \dot{Q}_{\text{ch}}^{\text{base}} - \dot{Q}_{\text{evap,VCR}}(\mathrm{x}) > 0 \tag{36}$$

$$P_{\text{el,grid}}(\mathrm{x}) = -\frac{\dot{W}_{net,OCR}(x)}{\eta_{\text{GER}}} + P_{el,ch}(x) + \frac{\dot{W}_{c,VCR}(x)}{\eta_{\text{GER}}} > 0 \tag{37}$$

For the sake of validation and comparison, the integrated and interconnected VCR-ORC superstructure for the factory utilities decarbonization is optimized using the MMHHO, as shown in Figure 5, which is an enhanced HHO with adaptive and diversification strategies, benchmarked against NSGA-II under identical settings [19].

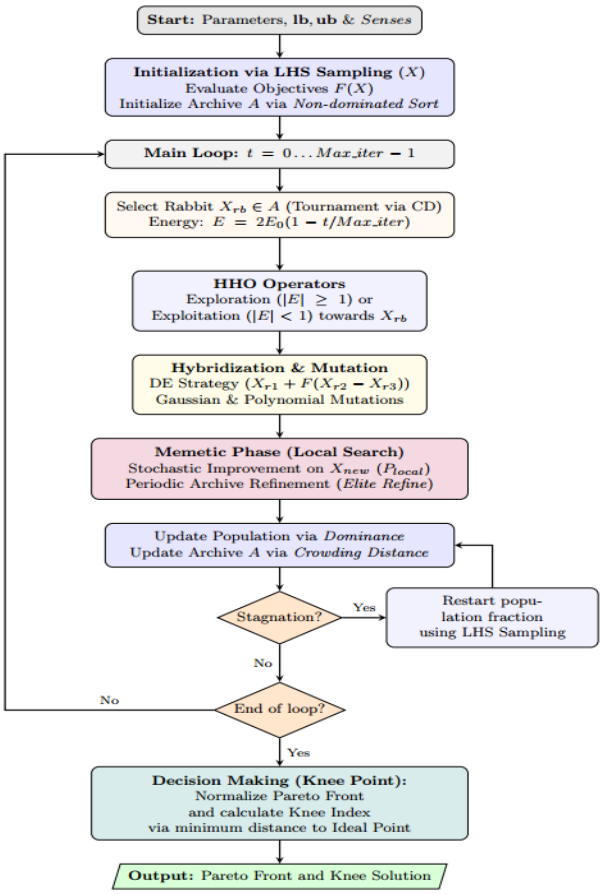

Figure. 5. *Flow chart of the optimization process by MMHHO.*

4. Results and Discussions

Both MMHHO and NSGA-II algorithms confirmed the robustness of the superstructure optimization framework. The Knee Point Solution (or Best Compromise) of the NSGA-II Pareto front achieves a $CO_{2,\text{avoided}} = 2{,}624.42$ t yr^{-1}, dominated by boiler decarbonization, with $\dot{C}_{\text{tot}} = 461.05$ USD h^{-1}, investment of 2.22×10^6 USD, annual savings of 4.56×10^5 USD yr^{-1} and $PB = 4.86$ years. MMHHO yields a superior solution with $CO_{2,\text{avoided}} = 2{,}668.53$ t yr^{-1}, $\dot{C}_{\text{tot}} = 460.78$ USD h^{-1} and higher savings $(4.63 \times 10^5$ USD yr$^{-1})$, maintaining $PB = 4.86$ years. This corresponds to a +1.68% increase in avoided emissions and −0.06% reduction in cost relative to NSGA-II, indicating improved performance. Both algorithms converge to a dominant configuration with >99% of the emission reduction in the boiler, highlighting electrification and exergy efficiency as decarbonization drivers. Overall, MMHHO improves convergence toward high-performance solutions, while NSGA-II preserves solution diversity, as is illustrated in Figure 6.

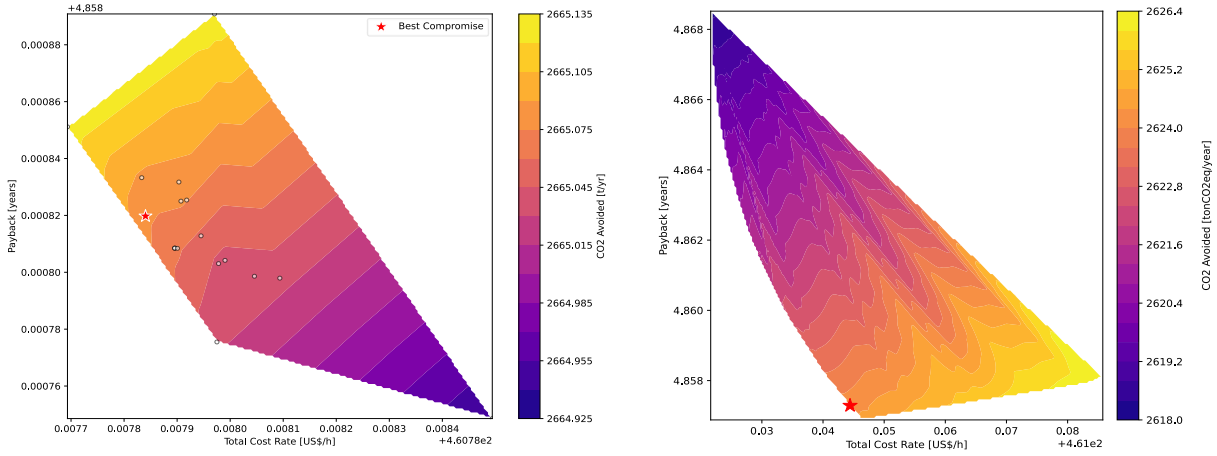

(a) (b)

Figure 6 *– MMHHO (a) and NSGA-II (b) 2D projections.*

The results show that the Knee Point Solutions obtained by MMHHO over 10 runs consistently converge to a well-defined optimal region, achieving robust performance, thus confirming the reliability and structural stability of the solutions, as shown in Table 1.

Table 1. *Statistical consistency of MMHHO results.*

Variable	**Mean**	**Median**	**Variance**	**Std. dev.**
$\Delta T_{evap,\mathrm{VCR}}\ (K)$	3.000	3.000	4.444e-05	0.007
$\Delta T_{\mathrm{cond,VCR}}\ (K)$	4.000	4.000	4.444e-05	0.007
$\dot{Q}_{\mathrm{cond,VCR}}\ (kW)$	1,439.12	1,439.15	0.357	0.598
$PP_{evap,\mathrm{ORC}}\ (K)$	5.810	5.810	1.333e-04	0.012
$PP_{cond,\mathrm{ORC}}\ (K)$	4.998	5.000	8.444e-05	0.009
$\dot{Q}_{\mathrm{cond},ORC}\ (kW)$	1,055.47	1,055.65	0.582	0.763
$\dot{C}_{\mathrm{tot}}\ (US\$.h^{-1})$	460.97	460.90	0.085	0.292
$\dot{CO}_{2,\mathrm{avoid}}\ (ton.yr^{-1})$	2,667.45	2,668.20	3.925	1.98
$PB\ (yr)$	4.874	4.870	4.489e-04	0.021

The MMHHO optimal compromise configuration defines a highly integrated system in which VCR and ORC systems operate synergistically and do not use heat exchangers. For the VCR, $\Delta T_{\mathrm{evap}} = 3.00$ K, $\Delta T_{\mathrm{cond}} = 4.00$ K, while the ORC operates with $PP_{\mathrm{evap}} = 5.81$ K, $PP_{\mathrm{cond}} = 5.00$ K. Thermodynamic results, in Tables 2 and 3, show that the VCR operates efficiently (COP = 6.053) and the ORC electric power contribution (178.19 kW) is relatively small, but contributing to the reduction of grid demand and the reduction of exergy destruction in the heat exchangers.

Table 2. *VCR subsystem performance after MMHHO optimization*

Parameter	Symbol	Value	Unit
Evaporator cooling load	$\dot{Q}_{evap,VCR}$	1,031.06	kW
Condenser heating load	$\dot{Q}_{cond,VCR}$	1,439.16	kW
Compressor electric power	$\dot{W}_{c,VCR}$	408.10	kW
Total COP	$COP_{tot,VCR}$	6.053	–
Cooling COP	$COP_{ref,VCR}$	2.526	–
Heating COP	$COP_{heat,VCR}$	3.526	–

The VCR system provides 1,031.06 kW of chilled water and 1,439.16 kW of hot water, representing 7.69% and 57.68% of the total cooling and heating demand, respectively, demanding only 408.10 kW of electricity.

Table 3. *ORC subsystem performance after MMHHO optimization*

Parameter	Symbol	Value	Unit
Evaporator heat demand	$\dot{Q}_{evap,ORC}$	1,234.02	kW
Condenser heating load	$\dot{Q}_{cond,ORC}$	1,055.83	kW
Turbine electric power	$\dot{W}_{t,ORC}$	187.64	kW
Pump electric power	$\dot{W}_{p,ORC}$	9.45	kW
Net electric power output	$\dot{W}_{net,ORC}$	178.19	kW
Electric efficiency	η_{ORC}	14.44	%

The ORC system supplies 1,055.83 kW of hot water to complete the remaining 42.32% of the total heating demand, while generating 178.19 kW of electricity. The natural gas demand of the boiler is only 1,402.30 kW, representing 47% of the current demand (2,982.78 kW), to supply 1,234.02 kW of steam to the ORC system.

Regarding electricity demand from the grid, the existing compression chillers demand 2,905.38 kW of electricity to produce most of the cooling demand (92.31%), i.e., 12,376.94 kW of chilled water. Despite the electrical demand of the VCR system (408.10 kW), due to the electricity generation in the ORC system (178.19 kW), the electricity demand from the grid is 3,147.40 kW, which is 1.41% lower than the current demand (3,192.38 kW).

Cost distribution in Figure 7(a) shows that grid electricity dominates the contribution, followed by natural gas, with smaller VCR and ORC contributions. Figure 7(b) shows that avoided CO_2 emissions are mainly in boiler.

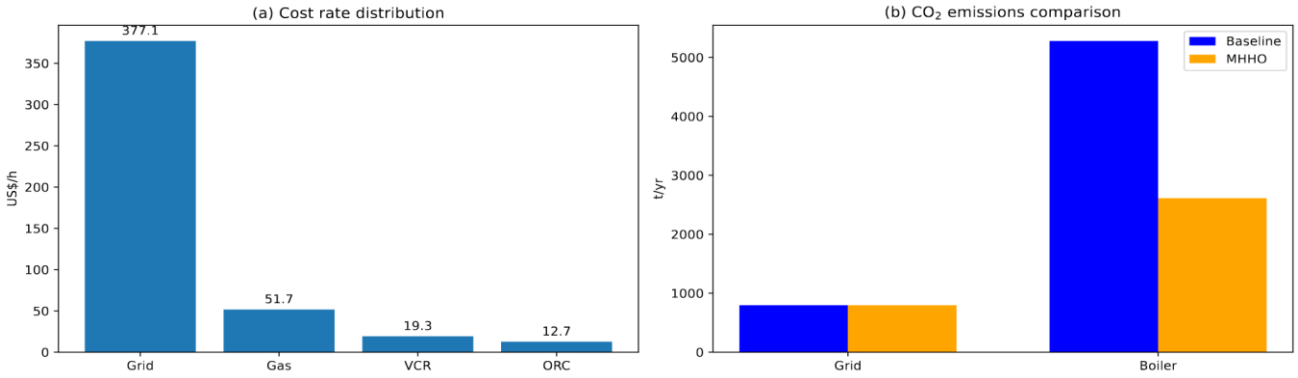

Figure. 7. *Results of the optimal* compromise *configuration obtained by MMHHO.*

Table 4 shows the boiler and grid emissions, comparing MMHHO configuration (new system) and the current configuration (baseline), considering the emission factor of natural gas (201.96 kg_{CO_2}/MWh) and the average of the lowest emission factors of the Brazilian grid, which occurred before 2011 and after 2022 (28.9 kg_{CO_2}/MWh).

Table 4. *Boiler and grid emissions*

Parameter	Symbol	Value	Unit
Boiler CO_2 emission (baseline)	$\dot{m}^{base}_{CO_2,boiler}$	5,280.66	$t \cdot yr^{-1}$
Boiler CO_2 (new system)	$\dot{m}^{new}_{CO_2,boiler}$	2,611.47	$t \cdot yr^{-1}$
Grid CO_2 emission (baseline)	$\dot{m}^{base}_{CO_2,grid}$	808.75	$t \cdot yr^{-1}$
Grid CO_2 emission (new system)	$\dot{m}^{new}_{CO_2,grid}$	797.35	$t \cdot yr^{-1}$

The results in Table 4 suggested a total decarbonization level of 55.97%. However, the radar analysis in Figure 8 reveals a clear subsystem hierarchy. The decarbonization is driven by thermal source (49.45% boiler emission reduction via VCR–ORC), while costs are dominated by grid electricity. The VCR acts as the main coupling element, and the ORC has a secondary role. This structural asymmetry shows emissions depend on thermal variables and costs on electricity, with feasibility governed by operational savings despite high investment.

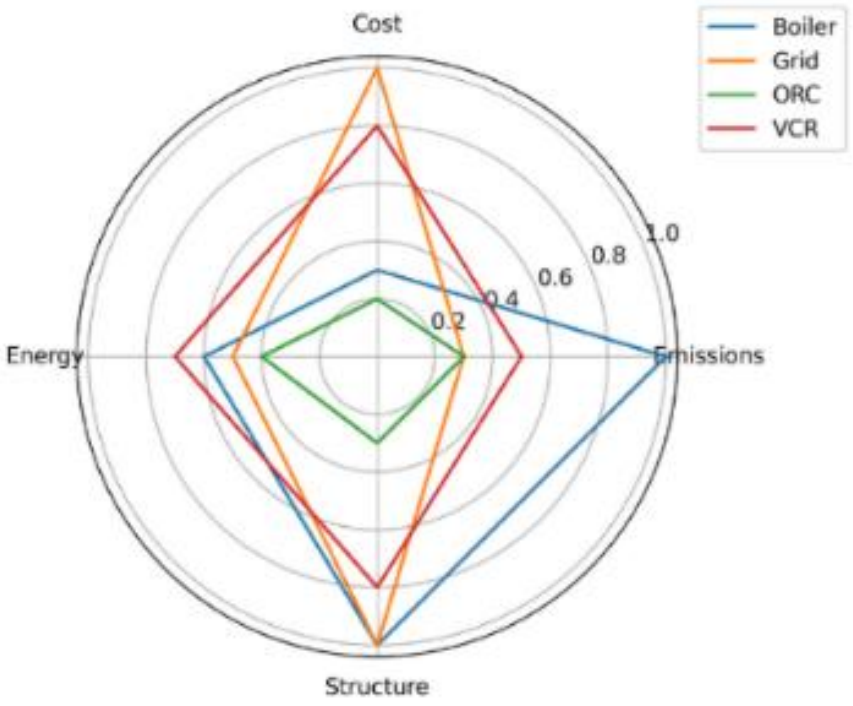

Figure. 8. *Radar representation of the structural contributions of trade off.*

5. Conclusions

Instead of using the methodology of defining scenarios, as done in a previous study that evaluated the decarbonization of the utilities of this same chocolate factory, for the sake of comparison, this work proposed a comprehensive multi-objective optimization of an integrated energy superstructure alternative system, combining VCR, ORC, and conventional existing thermal systems, using a MMHHO algorithm. The obtained results demonstrate that the proposed framework can identify a structurally consistent and thermodynamically efficient solution for this complex decarbonization problem, with excellent convergence toward a narrow optimal viable region, with ORC-VCR system as drivers for decarbonization.

The optimization simultaneously minimized total cost rate and simple payback, while maximizing avoided CO_2 emissions. The solution resulted in a combination of process electrification and ORC-VCR system, avoiding exergy destruction in the heat exchangers and combining cooling and heating production, in which the VCR system supplies 7.69% and 57.68% of the cooling and heating demand, respectively, and the ORC produces the remaining 42.32% of the heating demand, generating 5,36% of the electricity demand. The optimized new thermal system, with ORC-VCR, allowed to achieve a balance between investment and operational cost, environmental performance, energy and exergy efficiency, with a total capital cost of 2,250,000 US$, approximately, and a payback period below 5 years. The total energy demand (electricity and natural gas) and emissions reduction are of 26.32% and 46.14%, respectively, and the natural gas reduction amounts is 53%.

A comparison between the previous expert-based study and the current multi-objective optimization (MMHHO) reveals a strategic evolution in the factory's decarbonization pathway. The earlier research, based on scenario analysis, identified total electrification (Scenario C) as the most promising route. This approach required an investment of US$ 2,679,612.19 to achieve a 2.23-year discounted payback and the highest absolute emission reduction of 0.467 t/h of CO_2 (a 54% decrease). However, the current optimization using the MMHHO algorithm identifies a superior compromise solution at the knee point of the Pareto frontier, balancing three conflicting objectives more pragmatically. Although it presents a higher payback of 4.86 years, this configuration reduces the required capital investment to approximately US$ 2,250,000 and total CO_2 avoided is 30.5% $t.h^{-1}$ through the synergistic integration of an ORC-VCR system. While the empirical study targeted environmental extremes, the MMHHO compromise solution ensures annual savings of US$ 463,105 and maintains existing thermal assets. This provides operational and maintenance flexibility that total electrification would lack. Thus, the multi-objective approach defines a technical-economic limit where exergetic efficiency and industrial viability outperform the isolated pursuit of minimum emissions.

Acknowledgments

The authors acknowledge the support of the Federal Institute of Espírito Santo (IFES) and the Federal University of Espírito Santo (UFES), and of the Brazilian agencies CNPq and FAPES.

Nomenclature

Abbreviations

Symbol	Description
BM	Bare-module
CEPCI	Chemical Engineering Plant Cost Index
CRF	Capital recovery factor
EF	Emission factor
MMHHO	Multi-objective Harris Hawks Optimization
NSGA-II	Non-dominated Sorting Genetic Algorithm II
LHV	Lower heating value
ORC	Organic Rankine Cycle
VCR	Vapor Compression Refrigeration
PVT	Photovoltaic-thermal
TE	Energy tariff
TUSD	Distribution tariff
SIN	Brazilian interconnected grid

Greek symbols

Symbol	Description
ΔT	Temperature difference, K
ΔT_{pp}	Pinch-point temperature difference, K
ΔT_{evap}	Evaporator temperature difference, K
ΔT_{cond}	Condenser temperature difference, K
η	Efficiency, -
η_{ORC}	ORC efficiency, -
η_{boiler}	Boiler efficiency, -
η_{gen}	Generator efficiency, -
η_{is}	Isentropic efficiency, -
ρ	Density, kg m^{-3}
μ	Mean value, -
σ	Standard deviation, -

Roman symbols

Symbol	Description
A_{HX}	Heat exchanger area, m^2
BM	Bare-module factor, -
C	Capital cost, USD
$\dot{C}$	Cost rate, USD h^{-1}
C_{tot}	Total investment cost, US$
$\dot{C}_{tot}$	Total cost rate, USD.h^{-1}
$\dot{C}_{grid}$	Grid electricity cost rate, USD.h^{-1}
$\dot{C}_{gas}$	Natural gas cost rate, USD.h^{-1}
$\dot{C}_{fuel}$	Fuel cost rate, USD.h^{-1}
$\dot{C}_{el}$	Electricity cost rate, USD.h^{-1}
$\dot{C}_{sav}$	Annual cost savings, USD.tr^{-1}
C_{VCR}	Capital cost of VCR subsystem, US$
C_{ORC}	Capital cost of ORC subsystem, US$
C_{HX}	Heat exchanger cost, US$
$CEPCI$	Cost index, -
CF	Contingency factor, -
COP	Coefficient of performance, -
COP_{ch}	Chiller COP, -
CRF	Capital recovery factor, -
E	Annual electricity consumption, kW.yr^{-1}
E_{grid}	Grid electricity consumption, kW.yr^{-1}
EF	Emission factor, $\mathrm{kgCO_2.\,kWh^{-1}}$
f	Maintenance factor, -
h	Specific enthalpy, $\mathrm{kJ.kg^{-1}}$
i	Interest rate, -
r	Discount rate, -
LHV	Lower heating value, $\mathrm{MJ.kg^{-1}}$
$LMTD$	Logarithmic mean temperature difference, K
$\dot{m}_{steam}$	Steam mass flow rate, $kg.\mathrm{s^{-1}}$
$\dot{m}_{CO_2,boiler}$	Boiler emissions, $\mathrm{t.yr^{-1}}$

Subscripts and Superscripts

Symbol	Description
boiler	boiler
cond	condenser
evap	evaporator
grid	electrical grid
gas	natural gas
ch	chiller
c	compressor
e	expansor
p	pump
ORC	Organic Rankine Cycle

CV	Coefficient of variation, -

Roman symbols

Symbol	Description
$\dot{m}_{VCR}$	Refrigerant mass flow rate, $kg.\mathrm{s^{-1}}$
$\dot{m}_{ORC}$	Working fluid mass flow rate, $kg.\mathrm{s^{-1}}$
$\dot{m}_{fuel}$	Fuel mass flow rate, $kg.\mathrm{s^{-1}}$
$\dot{m}_{CO_2,avoid}$	Avoided emissions, $\mathrm{t.yr^{-1}}$
P_{ch}	Chiller power, kW
$\dot{Q}_{proc}$	Process heat demand, kW
$\dot{Q}_{boiler}$	Boiler heat duty, kW
$\dot{Q}_{cond}$	Condenser duty, kW
$\dot{Q}_{evap}$	Evaporator duty, kW
$\dot{Q}_{rec}$	Recovered heat, kW
PB	Payback period, years
PP	Pinch-point temperature difference, K
$\dot{V}_{gas}$	Gas flow rate, $m^3.h^{-1}$
$\dot{W}$	Mechanical power, kW
$\dot{W}_c$	Compressor power, kW
$\dot{W}_t$	Turbine power, kW
$\dot{W}_p$	Pump power, kW
$\dot{W}_{net}$	Net power output, kW
$\dot{W}_{c,VCR}$	VCR compressor power, kW
$\dot{W}_{t,ORC}$	ORC turbine power, kW
$\dot{W}_{p,ORC}$	ORC pump power, kW
$\dot{W}_{net,ORC}$	Net ORC power, kW
U	Heat transfer coefficient, $\mathrm{W.m^{-2}}.K^{-1}$
$x_{turb,out}$	Turbine outlet quality, -

Subscripts and Superscripts

Symbol	Description
VCR	Vapor Compression Refrigeration
proc	process
fuel	fuel
steam	steam
th	thermal
tot	total
net	net
base	baseline
new	optimized
avoid	avoided

References

[1] Hasanbeigi, A., & Price, L. (2012). A review of energy use and energy efficiency technologies for the textile industry. Renewable and Sustainable Energy Reviews, 16(6), 3648-3665.

[2] Zhang, X., Bu, Z., Lin, S., Chen, Z., Li, W., & Pei, Y. (2020). GeTe thermoelectrics. Joule, 4(5), 986-1003.

[3] Natarajan, S., Ghosh, K., & Srinivasan, R. (2012). An ontology for distributed process supervision of large-scale chemical plants. Computers & Chemical Engineering, 46, 124-140.

[4] Yee, T. F., & Grossmann, I. E. (1990). Simultaneous optimization models for heat integration—II. Heat exchanger network synthesis. Computers & chemical engineering, 14(10), 1165-1184.

[5] Arpagaus, C., Bless, F., Uhlmann, M., Schiffmann, J., & Bertsch, S. S. (2018). High temperature heat pumps: Market overview, state of the art, research status, refrigerants, and application potentials. Energy, 152, 985-1010.

[6] Quoilin, S., Van Den Broek, M., Declaye, S., Dewallef, P., & Lemort, V. (2013). Techno-economic survey of Organic Rankine Cycle (ORC) systems. Renewable and sustainable energy reviews, 22, 168-186.

[7] Colonna, P., Casati, E., Trapp, C., Mathijssen, T., Larjola, J., Turunen-Saaresti, T., & Uusitalo, A. (2015). Organic Rankine cycle power systems: from the concept to current technology, applications, and an outlook to the future. Journal of Engineering for Gas Turbines and Power, 137(10), 100801.

[8] Tian, Y., Huang, Z., Li, X., & Tian, J. (2022). Parallel-connected battery module modeling based on physical characteristics in multiple domains and heterogeneous characteristic analysis. Energy, 239, 122181.

[9] Walmsley, T. G., Atkins, M. J., Walmsley, M. R., Philipp, M., & Peesel, R. H. (2018). Process and utility systems integration and optimisation for ultra-low energy milk powder production. Energy, 146, 67-81.

[10] Walmsley, T. G., Atkins, M. J., Walmsley, M. R., & Neale, J. R. (2016). Appropriate placement of vapour recompression in ultra-low energy industrial milk evaporation systems using Pinch Analysis. Energy, 116, 1269-1281.

[11] Aghaei, A. T., & Saray, R. K. (2021). Optimization of a combined cooling, heating, and power (CCHP) system with a gas turbine prime mover: A case study in the dairy industry. Energy, 229, 120788.

[12] Deb, K., Pratap, A., Agarwal, S., & Meyarivan, T. A. M. T. (2002). A fast and elitist multiobjective genetic algorithm: NSGA-II. IEEE transactions on evolutionary computation, 6(2), 182-197.

[13] Gonçalves, A. N., Fonseca, F. M., Morawski, A. P., de Faria, P. R., & Santos, J. J. C. S. (2025). 4E comparative analysis of energy transition scenarios for the decarbonization of a chocolate factory utilities in Brazil. Frontiers in Chemical Engineering, 7, 1716804.

[14] Qin, P., Liao, M., Zhang, D., Liu, Y., Sun, J., & Wang, Q. (2019). Experimental and numerical study on a novel hybrid battery thermal management system integrated forced-air convection and phase change material. Energy Conversion and Management, 195, 1371-1381.

[15] Rocha, H. R., Honorato, I. H., Fiorotti, R., Celeste, W. C., Silvestre, L. J., & Silva, J. A. (2021). An Artificial Intelligence based scheduling algorithm for demand-side energy management in Smart Homes. *Applied Energy*, *282*, 116145.

[16] Index, P. C. (2021). *Chemical Engineering Magazine*.

[17] Bejan, A., Tsatsaronis, G., Moran, M., 1996. Thermal Design and Optimization, Wiley

[18] Wang, G. Y., Li, Y. P., Liu, J., Huang, G. H., Chen, L. R., Yang, Y. J., & Gao, P. P. (2022). A two-phase factorial input-output model for analyzing CO2-emission reduction pathway and strategy from multiple perspectives–A case study of Fujian province. Energy, 248, 123615.

[19] Heidari, A. A., Mirjalili, S., Faris, H., Aljarah, I., Mafarja, M., & Chen, H. (2019). Harris hawk's optimization: Algorithm and applications. Future generation computer systems, 97, 849-872.